Design Concept of an Integrated Vision System for Cost-effective Part-Presentation

Kok-Meng Lee
Associate Professor.

The George W. Woodruff School of Mechanical Engineering, Georgia Institute of Technology, Atlanta, GA 30332-0405

The cost of feeding parts to a robot for either machine loading or for assembly has been recognized as excessively expensive. The lack of a cost-effective generic part-presenter has prevented the flexibility of the overall manufacturing automation to be fully exploited. For this reason, the design concept of an integrated microprocessor-controlled vision system based on retroreflective vision sensing has been developed at the Material Handling Research Center in Atlanta. Where the orientation of a part can be characterized by its silhouette, outline, or structured "engineering landmarks," the concept of using retroreflective materials in vision-guided part-presentation system has been proven to have significant potential for improving reliability, reducing computation, and lowering implementation cost.

This paper presents optic design concepts for collocated illumination for cost effective part-presentation. The design concepts are illustrated with practical applications and experimental results. The uniformity of the image irradiance across the sensor surface, in general, depends on several factors such as the intensity distribution of the light source, the reflectance characteristics of the object and background, and the geometrical relationship between the imaging sensor, the illumination source, and the target. The trust of this paper focuses on the analytical model which characterizes the influences of these factors for optic design of retroreflection. This engineering basis is not only necessary for developing practical yet potentially cost-effective optic design concepts, but also provides a useful tool for performance prediction to drive the design for vision-guided part-presentation.

1 Introduction

Even though machine vision can add considerably to flexibility by simplifying grippers, component feeders, and location tooling, and can reduce engineering time for system implementation, vision system applications for part verification, kitting, and presentation for robot assembly have been limited. Two major problems often associated with the use of machine vision are poor reliability and excessive image processing time. Both of these depend on the illumination technique, the complexity of the geometry, and the surface reflectance of both the background and the objects to be handled.

Illumination and its measurements are, perhaps, among the least understood technologies. Discussion and communication of desired operating parameters of optics are complicated by a plethora of nomenclatures for seemingly similar units of measurements. Furthermore, system specifications for illumination are often vague and left to the final user. As a result, illumination deficiencies must often be compensated for with expensive digital hardware/software. When illumination deficiencies become apparent, it is then that critical light parameters such as luminous intensity, illumination uniformity, spectral output, and image spectral irradiance become an unwelcome part of our vocabulary. Direct symptoms of an unfit light source are not only long exposure times, but can also include inaccurate image characteristics due to nonuniform illumination. The uniformity of the image irradiance across the sensor surface depends on several factors: the intensity distribution of the light source, the reflectance characteristics of the object and background, and the geometrical relationship between the imaging sensor, the illumination source, and the target.

Retroreflection is not commonly found on the surfaces of most objects which exhibit a combination of diffuse and specular reflection. The ideal retroreflector returns the incident radiation in the direction of its arrival. Elsewhere the author and his coworkers describe the concept of retroreflective vision sensing for generic part presentation [1] and its application to flexible part-feeding for assembly automation [2] [3]. Retroreflective vision sensing improves vision realiability, reduces computation, and lowers implementation cost by providing a reliable contrast between the object and its background regardless of the surface reflectance.

Special retroreflective materials have widely been used in traffic control and safety sign on highways and airports [4]

Contributed by the Production Engineering Division for publication in the JOURNAL OF ENGINEERING FOR INDUSTRY. Manuscript received July 1991; revised Jan. 1993. Associate Technical Editor: S. G. Kapoor.

[5] [6]. Retroreflector material has also been used as a non-contact position sensor of a large space structure [7] and more recently, in field tracking of automated guided vehicles (AGV) [8]. Using unique features of retroreflective materials as a cost-effective means for presenting parts to robots, the orientation of which can be determined from the silhouette or by modifying part design to include "landmarks," was conceptualized by Lee et al. [1]. The basic principle of retroreflective vision sensing for part-presentation is the use of retroreflective surfaces to maximize the ability of a vision system to reliably and quickly locate parts. One way is to make the surface of a parallel retroreflective so it appears much brighter than objects on it. Alternatively, retroreflective landmarks can be intentionally created on objects to aid in location tracking. Since the retroreflective material has a distinctive surface reflectance that is not commonly found in natural or man-made objects, it enables reliable digital images with high object-to-background contrast to be obtained without a prior knowledge of object geometry and surface reflectance. The location and orientation of the part can then be determined with relatively simple, high-speed computation without the need for a detailed reflectance map of the part.

In order to establish an engineering basis for cost-effective vision-guided part-presentation, this paper presents the optic design concepts for flexible part-feeding applications. The design concepts have been developed on the basis of retroreflective vision sensing. The remainder of the paper is organized as follows: The fundamental equations of optics for retroreflection are presented in Section 2. Then optic design concepts and the sensitivity of the operational parameters to image characteristics are described, followed by a presentation of illustrative applications. Finally, conclusions are drawn and further work is suggested.

2 Fundamental Equations of Optics

Consider an optical aperture located at a distance f from the image plane as shown in Fig. 1(a). The solid angle of the cone of rays leading to the patch on the object is equal to that corresponding patch in the image [9].

$$\frac{\delta O}{\delta A_i}=\frac{\cos\theta}{\cos\beta}\left[\frac{D'}{f}\right]^2 \tag{1}$$

where

δO = patch area of the object surface,
δA_i = patch area on the image,
β = an angle between a light ray and the surface normal, and
θ = an angle between a light and the optical axis.

The amount of light radiated from a surface is called the radiance which is the power per unit area per unit solid angle ($W.m^{-2}.sr^{-1}$—watts per square meter per steradian). Thus, the power of the light originating on the patch and passing through the lens is

$$\delta P = L\,\delta O\,\Omega\cos\beta \tag{2}$$

where

Ω = solid angle subtended by the lens as seen by the patch, and
L = radiance of the object patch δO in the direction toward the lens.

The amount of light falling on a surface is called the irradiance I or the power per unit area (W/m^2—watts per square meter) incident on the surface. The irradiance of the image at the patch under consideration is given by $I = \delta P/\delta A_i$. Substituting of δO from Eq. (1) into Eq. (2), the irradiance of the image is given by

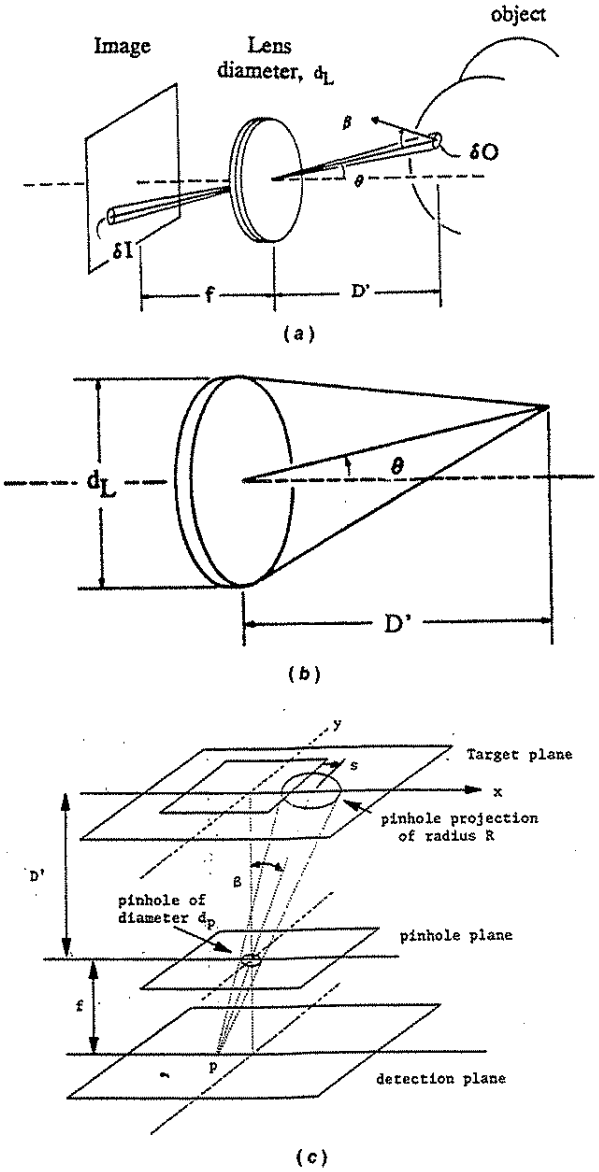

Fig. 1 Fundamental of optics (*a*) relationship between image irradiance and the radiance of object surface (*b*) solid angle of lens optics (*c*) solid angle of pinhole optics

$$\frac{I}{L}=\Omega\left[\frac{D'}{f}\right]^2\cos\theta \tag{3}$$

Equations (1)–(3) are valid for a pin hole as well as a lens of diameter d_L as shown in Fig. 1(a) since rays passing through the center of the lens are not affected. The solid angle that the lens subtends when viewed from the light-emitting surface is illustrated in Fig. 1(b). Figure 1(c) illustrates the solid angle for the case of a pin-hole. Thus, the solid angle can be expressed by Eq. (4):

$$\Omega=\frac{\pi}{4}\frac{d_L^2\cos\theta}{(D'/\cos\theta)^2}. \tag{4}$$

For a pin-hole, $d_L = d_p$ where d_p is the diameter of the pin hole. Equation (3) leads to

$$\frac{I}{L}=\frac{\pi}{4}\frac{\cos^4\theta}{F^2} \tag{5}$$

where

$$F=\begin{cases} f/d_L & \text{for a lens} \\ f/d_p & \text{for a pin hole.} \end{cases}$$

Scene radiance depends on the amount of light that falls on a surface, the fraction of the incident light that is reflected, and the geometry of light reflection. In other words, the radiance of a surface, L, generally depends on the direction from which it is viewed as well as on the direction from which it is illuminated. The radiance of the retroreflective sheeting is typically characterized by the coefficient of reroreflection $R'(\alpha,\beta)$ [5] which is defined as follows:

$$R'(\alpha,\beta)=\frac{I_r}{EA_r} \tag{6}$$

where

I_r = luminous intensity of the retroreflector in the direction of observation in watts/sr, candela, or lm/sr.
E = illuminance at the retroreflector on the plane perpendicular to the direction of the incident light in Lux,
A_r = retroreflecting surface area, m^2,
α = observation angle which is the angle between the observation axis and incident light ray, and
β = entrance angle which is the angle between the surface normal of the target plane and the incident light.

The coefficient of retroreflection of a typical retroreflective sheeting is displayed in Figs. 2(*b*) and 2(*c*) as a function of observation and entrance angles, respectively, where the nomenclature is defined in Fig. 2(*a*). Within an angle of 0.2 deg. from the principle axis of incident light, typical retroreflective sheeting will reflect with over 250 times the intensity of a typical diffuse white surface.

Consider an incident light from a spectral illuminator of wavelength λ falls on a retroreflective sheeting characterized by the coefficient of retroreflection $R'(\alpha,\beta)$. Since

$$L=R'(\alpha,\beta)\frac{E_s(\phi)}{(D/\cos\phi)^2} \tag{7}$$

where $E_s(\phi)$ is the illuminous intensity distribution of the spectral illuminator; ϕ is the angular displacement of an incident light measured from the optical axis of the source; and D is the illumination distance defined in Fig. 2(*a*). Thus, the image irradiance can be expressed as

$$I=\frac{\pi}{4}\frac{E_S(\phi)R'(\alpha,\beta)}{F^2\,(D/\cos\phi)^2}\cos^4\theta. \tag{8}$$

The linearity of the gray-scale response of an imaging sensor is specified by an exponent "gamma γ."

$$M=KE^{\gamma} \tag{9}$$

where E is the time integral version of image irradiance, K is a constant, and M is the amplitude of the sensor output signal. A gamma of unity yields a linear response, whereas less than unity compresses the bright end of the response curve and greater than unity compresses the dark end. Many video imaging sensors have gamma of less than unity to compensate for video monitors that exhibit the opposite effect. Thus, the output signal of the imaging sensor element is of the form

$$M=K\left[\tau\frac{E_s(\phi)R'(\alpha,\beta)}{F^2\,(D/\cos\phi)^2}\cos^4\theta\right]^{\gamma}, \tag{10}$$

where τ is the effective exposure time. Equation (10) provides an analytical model for predicting the output signal corresponding to a retroreflective patch in terms of the following parameters: coefficient of retroreflection, illumination intensity distribution, and geometry. The applications of the analytical model to design cost-effective optic systems for use with retroreflective vision sensing and to predict the sensitivity of the parameters on the image characteristics are discussed in Section 3.

3 Pinhole Optic Design for Retroreflection

Lenses are often used with a camera to gather light reflected from (or emitted by) the object, to magnify the field-of-view, and to improve the image quality. However, actual lenses tend to introduce certain geometrical distortion in the image. The factors which limit the accuracy of dimensional measurements made with simple machine vision are the nonlinearity of the lens and the state of focus. The ability of retroreflective vision sensing to generate a high contrast digital image with relatively low illumination intensity offers the potential of eliminating the need of lenses for light-gathering. In addition to the simplicity of the pinhole design, pinhole, optics offer freedom from the geometrical distortion and virtually infinite depth of field.

Consider a point P on the detector plane as shown in Fig. 1(*c*). The radius of the pin-hole projection from the point P on the target plane can be derived from the geometry to be

$$\frac{R}{D'}=\frac{1}{2F}\left(1+\frac{f}{D'}\right).$$

The intensity of the point P on the detector is proportional to the overlapping area between the pinhole projection and the bright area on the target plane. The highest and lowest intensities, I_{max} and I_{min}, are corresponding to the cases when the pinhole projection is completely covered by the bright and dark areas, respectively. If δO is the area of pin-hole projection and δA is the portion of the object patch which reflects light into the dectector, then

$$\frac{\delta A}{\delta O}=1-\frac{1}{\pi}\left[\cos^{-1}S-S\sqrt{(1-S^2)}\right] \qquad |S|\le 1, \tag{11}$$

where $S = s/R$ and the displacement s is measured from the edge between the dark and bright areas to the center of the pinhole projection along the x-axis on the target plane. Since s is given by

$$s=x-D'\tan\beta_O$$

where β_O is the entrance angle defined at the edge on the target plane. The normalized distance S can be expressed as a function of β as follows:

$$S=\frac{D'}{R}(\tan\beta-\tan\beta_O). \tag{12}$$

The image irradiance model which describes the normalized output signal of the imaging sensor along the x-axis can be used to characterize the edge location. By noting that the intensity of the point P on the detector is proportional to $\delta A/\delta O$, the image irradiance model along the x-axis on the target plane can be expressed as:

$$M=K\left[\tau\frac{E_s(\phi)R'(\alpha,\beta)\cos^4\theta}{F^2(D/\cos\phi)^2}\frac{\delta A}{\delta O}\right]^{\gamma}. \tag{13}$$

The constraint imposed by the small lateral distance d, where d is the distance between the illumination source and the optical center as shown in Fig. 2(*a*), limits physical design and the heat generation of the illuminator. Unlike general purpose light sources which have a wide angular range of illuminance for uniform lighting on the factory floor, the illuminator for the retroreflector is designed to have a relatively narrow anglular range of illuminance, generally no more than that required for the field-of-view (FOV). For a given array size of a CCD or CID detector, the FOV is defined as the cone angle of the directions encompassed by the scene being imaged and is given by

Table 1 Comparison between three spectral light sources

Source	Wavelength (nm)	Unit Cost ($)	Life	Power
LED lamps	570-630	1.00	5,000,000 hours (MTBF)	100 mW
Laser Diode	790-840	200.00	250,000 hours (MTTF)	1 W (peak pulse power)
Xenon flash-tubes	830-1000	10.00	1,000,000 flashes (0.3-4 flashes/sec)	25 W (500 V nominal)

$$\text{FOV} = \pm\tan^{-1}\frac{1}{2}\frac{W}{D} = \pm\tan^{-1}\frac{1}{2}\frac{w}{f} \tag{14}$$

where W and w are the diagonal dimension of the FOV and the detector, respectively. As discussed by Lee et al. [1], it is desired that the collocated source be chosen to have a spectral characteristic which is distinctive from the general ambient lighting and be optimal for the photodetector response. Table 1 offers a comparison of three typical light sources for retroreflection; namely light-emitting diode (LED) [10], laser diode [11], and Xenon flashtubes [12].

Two illumination concepts are demonstrated for pin-hole optics. In order to investigate the influences of the optic parameters on image characteristics, the design is simulated using the optical model given above. The simulated target is a flat encapsulated glass-bead retroreflective sheeting. The characteristics of the simulated retroreflective sheeting are shown in Figs. 2(*b*) and 2(*c*) which were calibrated for 3M Scotchlite 3870 using computer photometry by the manufacturer (3M Traffic Control Material Division, St. Paul, MN). The coefficient of retroreflection, as shown in Figs. 2(*b*) and 2(*c*), can be represented by the following polynomial:

$$R'(\alpha, \beta = -4^\circ) = \sum_{i=0}^{10} a_i(\alpha/2)^i,\ 0 \le \alpha \le 2^\circ.$$

The coefficients (a_i, i = 0, . . . , 10) are 3.548E3, 2.419E2, −4.023E3, −6.919E4, 5.954E5, −2.131E6, 4.429E6, −5.763E3, 4.642E6, −2.117E6, and 4.172E5. The coefficient of retroreflection as a function of entrance angles for α = 0.2° is approximated by

$$R'(\alpha = 0.2^\circ, \beta) = 297.97 + 1.1208\,\beta - 0.0882\,\beta^2 \tag{16}$$

where

$$5^\circ \le \beta \le 65^\circ.$$

The LED spectral characteristic used in the computation is shown in Fig. 3 [10]. The luminous intensity ranges from 2.9 to 8.4 candles for the LED with typical values of 4.0 candles. The maximum junction temperature of the LED is limited to 110°C.

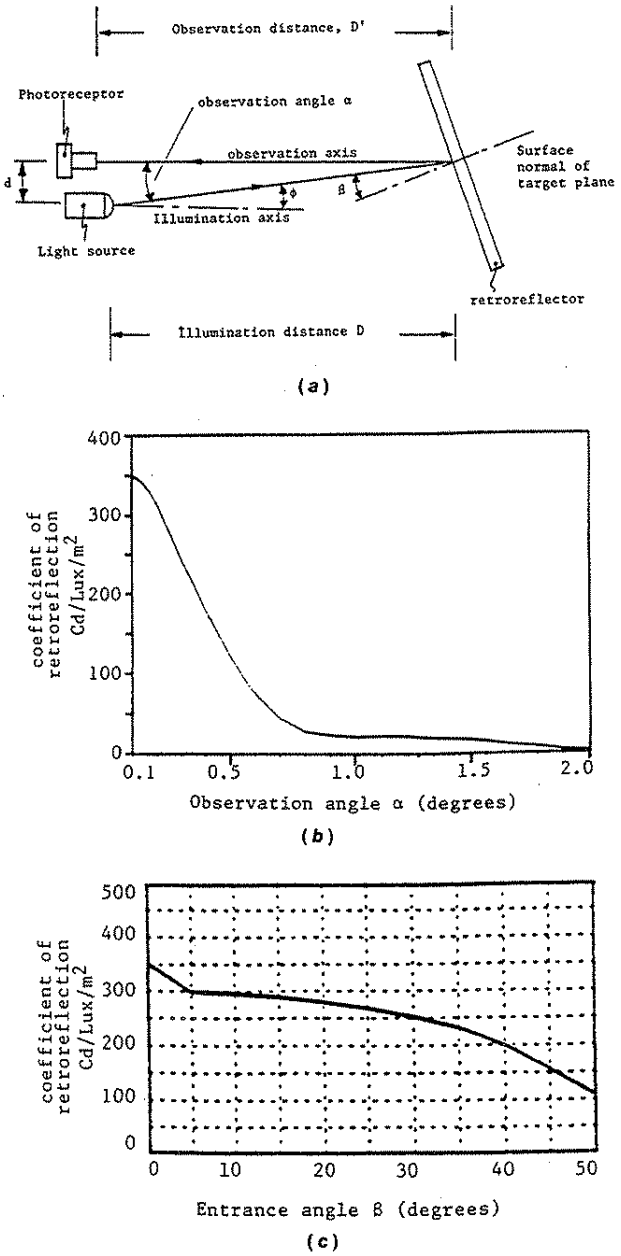

Fig. 2 Typical characteristics of retroreflection (a) nomenclature of retro-reflection measurement (b) coefficient of retroreflection as a function of observation angles (c) coefficient of retroreflection as a function of entrance angles

3.1 Optical Design I. Figure 4(*a*) illustrates a collocated illumination scheme for imaging small components (size less than 12 mm), which combines a beam splitter with a single high intensity LED. A beam splitter is an optical component that has the property of reflecting some portion of the light that strikes it and transmitting the remainder. Beam splitters appear transparent and are generally spectrally nonselective. A typical ratio of transmission-to-reflectivity is 50 percent/50 percent. Although the effective illumination efficiency of the scheme is 25 percent, the beam splitter which transmits illumination along the same optic axis allows small parts to be observed by the imaging sensor at a relatively short observation distance.

As shown in Eq. (8), the image irradiance is inversely proportional to the square of the illumination distance D. Other parameters shown in Fig. 4(*b*), which could significantly influence the image characteristics, are

ϵ = angle of misalignment between the observation and illumination axes,
ϕ = angular displacement of light ray measured from the illumination axis, and
δ = viewing angle.

The influences of these parameters on image characteristics are illustrated as follows:

Figure 5(*a*) presents the computed result of Eq. (10) for several different gamma values, where the relative sensor outputs are plotted as a function of entrance angles for δ = 90°, ϵ = 0°. As shown in the computed results, the effects of sensor nonlinearity and nonuniform illumination distribution can be reasonably well characterized by the following model:

$$\frac{M}{M_{\max}} = \frac{1}{1 + a(\tan^2\beta)}. \tag{17}$$

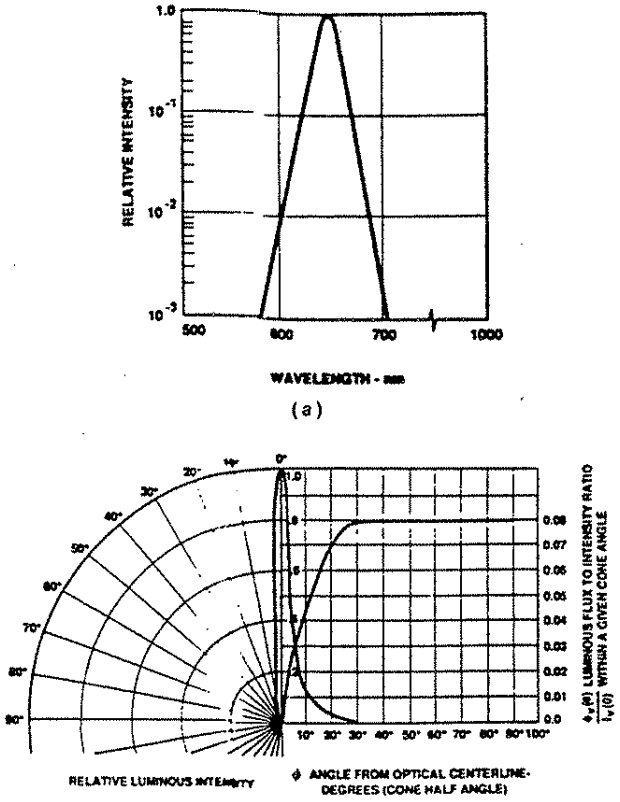

(a)

(a)

Fig. 3 AiGaAs LED characteristics [9] (*a*) relative intensity vs wavelength (*b*) relative luminous intensity vs angular displacement

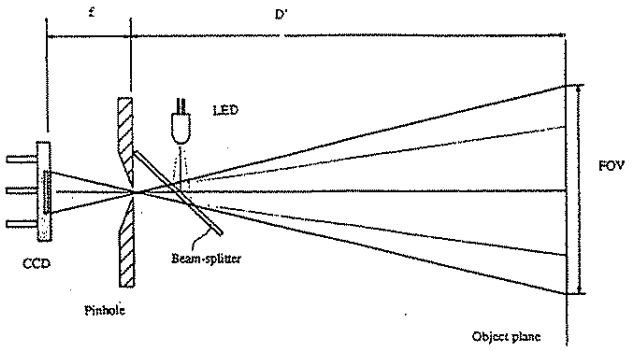

(b)

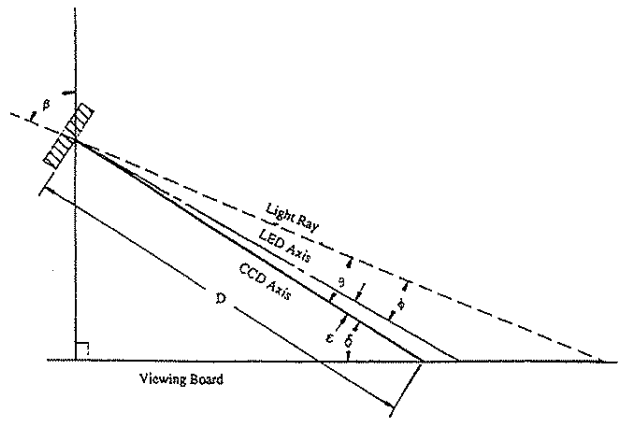

(b)

Fig. 4 Optic design example 1(*a*) schematics (*b*) illustration of parameters

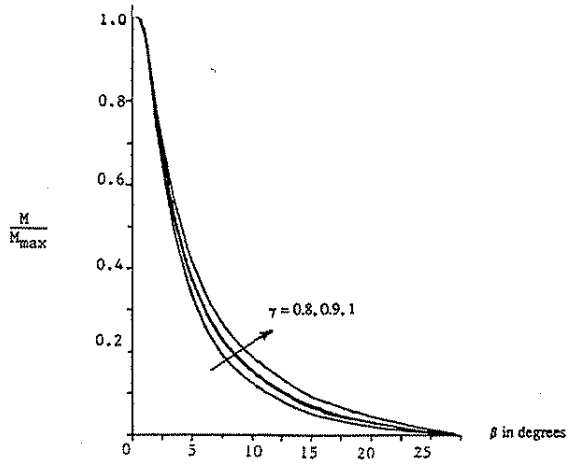

(a)

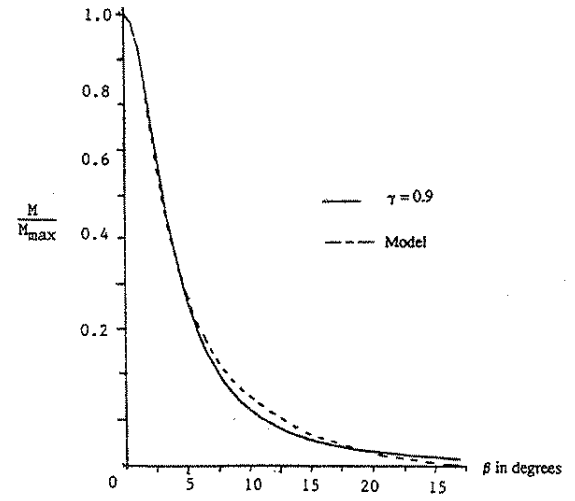

(b)

Fig. 5 Effect of sensor linearity ($\delta = 90°$, $\epsilon = 0$, $\theta = \phi$) (*a*) relative sensor output vs entrance angle (*b*) model

Figure 5(*b*) compares the model ($a = 230$) with the computed result for $\gamma = 0.9$. Since ($\tan \beta$) is linearly proportional to the radius of the illumination projection on the target plane, the model given by Eq. (17) indicates that illumination nonuniformity has a similar effect on greyscale computation as the geometrical radial distortion introduced by a typical lens.

As shown in Fig. 6, the illumination nonuniformity has a significant effect on the threshold selection as well as the image irradiance model which describes the normalized intensity along a path penpendicular to an edge, as given by Eq. (13). For a nonuniform source, the image irradiance model, in general, is location dependent. The effects of the misalignment angle ϵ and the viewing angle on illumination nonuniformity are shown in Figs. 7 and 8, respectively.

3.2 Optic Design II. For relatively large components (typical component size of 150 mm), the use of a single wide angle LED to achieve a desired image intensity is likely to require a long exposure time. An alternative scheme using multiple LEDs arranged in circular rings around a pin-hole is shown in Fig. 9(*a*), along with the geometrical parameters illustrated in three-dimensional space in Fig. 9(*b*).

The constraint imposed by the small lateral distance, $d = (dx^2 + dy^2)^{0.5}$, limits the maximum number of LEDs which can be effectively packed around the pin-hole. Figures 10–12 present the computed results using a design where twelve LEDs

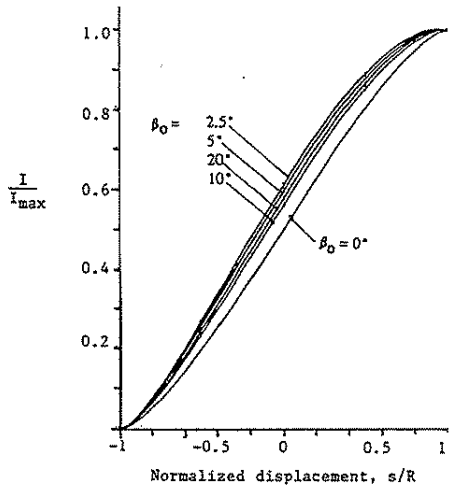

Fig. 6 Effect of nonuniformity on edge detection ($\delta = 90°$, $\epsilon = 0$)

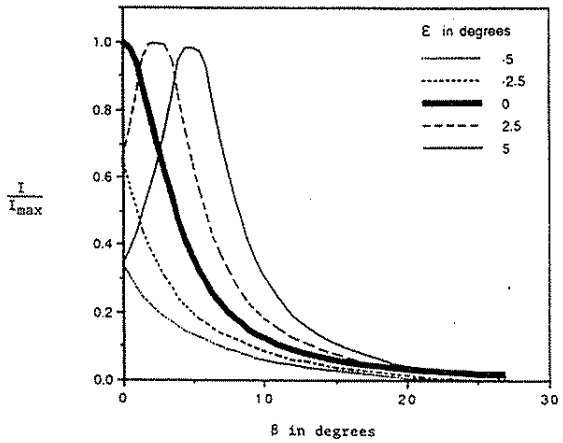

Fig. 7 Effect of misalignment between illumination and observation axes ($\delta = 90°$)

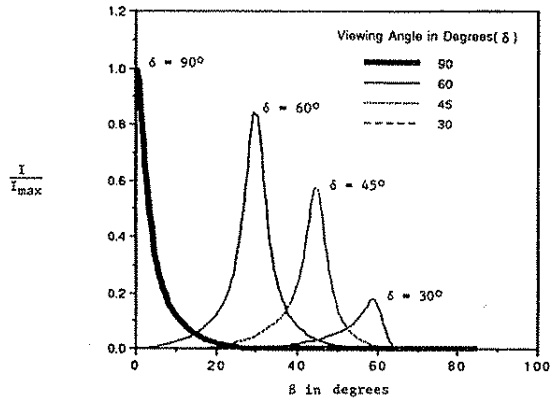

Fig. 8 Effect of viewing angles δ ($\epsilon = 0$)

are arranged at the vertices of two regular hexagons with the nominal radii of 6 mm and 12 mm. Equations (15) and (16) were used to characterize the targeted retroreflective surface in the simulation with the observation angle of $\alpha = 0.2°$.

In Fig. 11, the LED spread factor indicates the relative spacing between the adjacent LEDs from the nominal design which is characterized by a spread factor of unity. The design trade-off is clearly between overall uniformity and absolute intensity, both of which depend on the spread factor and the

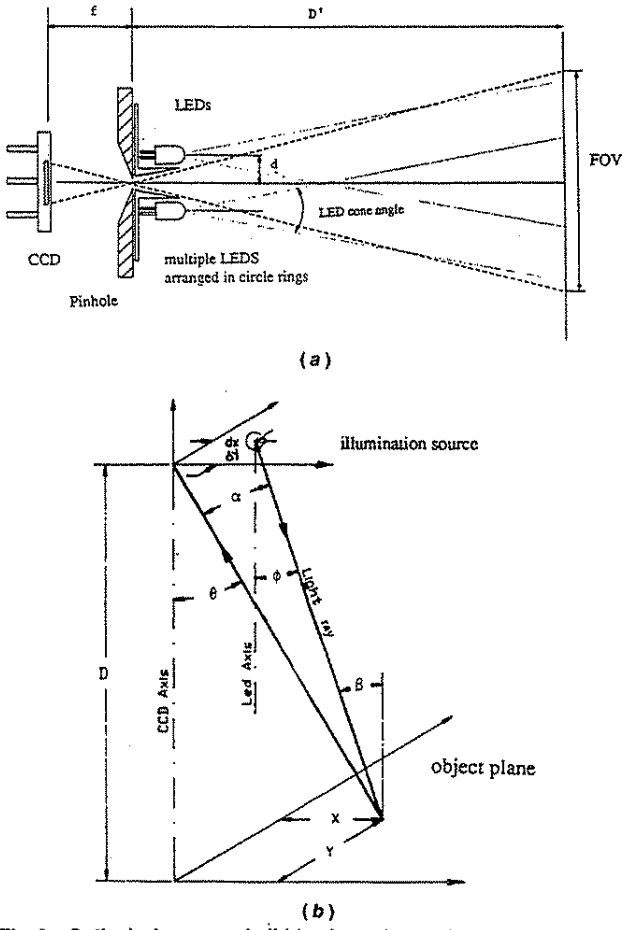

Fig. 9 Optic design example II (*a*) schematics (*b*) illustration of parameters

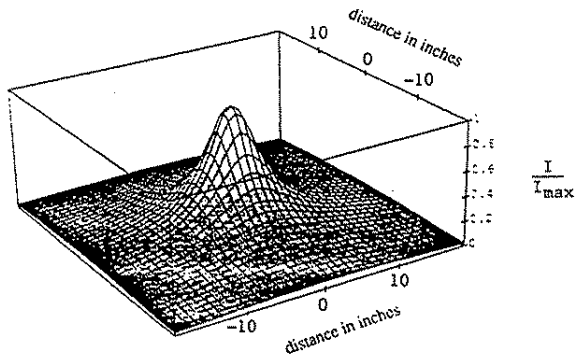

Fig. 10 Effects of LED illuminous intensity distribution

cone angle of the LEDs. However, for a given LED arrangement at a nominal radius, there exists an optimal observation distance with respect to both illumination uniformity and intensity as demonstrated in the simulated results in Fig. 12. The optimal viewing distance for the particular design occurs at approximately 36 inches.

4 Illustrative Applications

Retroreflective materials can be used as background in part-presentation or as a landmark on parts. The choice clearly depends on the part design and manufacturing process as reported by the author and his coauthor [1]. If the orientation of a part can be characterized by a two-dimensional object

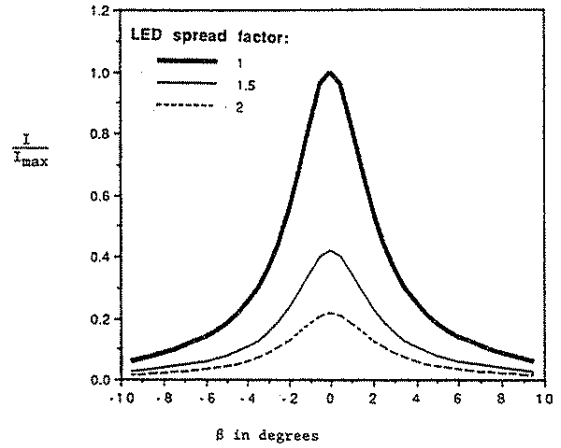

Fig. 11 Effects of relative LED spacing

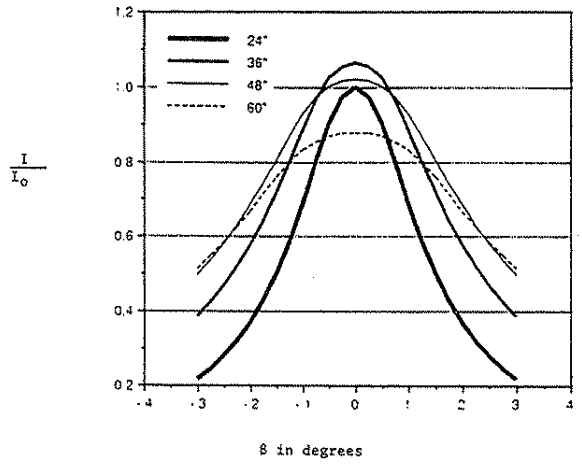

Fig. 12 Effects of observation distance (I_o = I_{max} at 24 in.)

silhouette, the retroreflective materials can be used as a background in generic part-presentation. In order to eliminate the need to apply retroreflective materials on each of individual trays, it is desired that a generic egg-crate-style tray be transparent such that when it is placed on a retroreflective surface, the object will appear as a dark silhouette against a reliable bright-field background. The concept feasibility was demonstrated experimentally using an integrated vision system [13] which allows a Motorola 68000 micro-processor (μP) to have direct control of the Texas Instruments charge-coupled-device (CCD).

4.1 Illustrative Example 1: Small Component Imaging. Small components (typically less than 10 mm) are often kitted in a egg-crate-style waffle pack for assembly. The pack may contain all the components necessary to assemble one product. Since the pack can be identified by the cell controller either by a bar code on the pack itself or by a bar-coded label stuck on the base assembly component, the pack may handle many components for several varieties of the same product.

Figure 13(*a*) shows an example where small electrical components are placed in hemispherical pockets of a typical egg-crate-style transparent plastic tray. Using the hemispherical pockets (1 inch diameter), the objects are positioned approximately in the center of the packet due to gravity. As a result, the object are viewed at a close distance with low power illumination since each of these small components require only a relatively small field-of-view of imaging.

The optic design I consisting of a 50 percent/50 percent beam splitter with a single narrow-angle LED as shown in Fig.

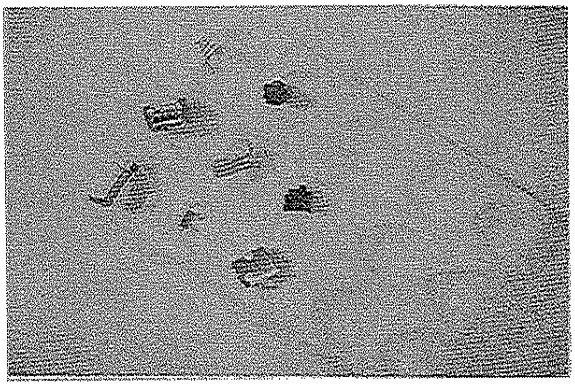

Fig. 13(*a*) Example images of typical small components in transparent trays

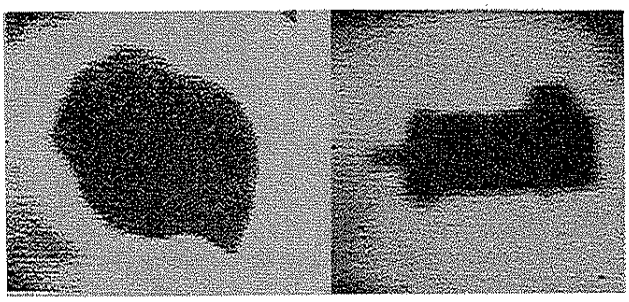

Fig. 13(*b*) Illustrative images of pin-hole optics

4(*a*) was used with a 0.1 mm diameter pin-hole to investigate the feasibility for these applications. Example images which were taken with the beam-splitter 6 inches vertically above the object surface are displayed in Fig. 13(*b*).

4.2 Illustrative Example 2: Machine Component Imaging. Backlighting (direct illumination of the background) has commonly been used to create a good contrast between the object and its background in part-presentation. However, this approach cannot be used with nontransparent trays. This restriction has severely limited backlighting for applications where the use of low-cost reusable trays or a conveyor for feeding parts is an advantage, since it is generally very costly (if not impossible) to keep the reusable surface of the tray transparent. On the other hand, retroreflective materials can be painted on trays. Thus, the techniques described in this paper can be used with nontransparent trays in order to create a reliable object-to-background contrast. The following example illustrates such an application.

Figure 14(*a*) shows a typical example if two machine components. The object on the left is a typical component prior to machine processing, its surface reflectance is "dull" or diffuse. The object on the right is a partially machined component of the same type, which has several "mirror-like" machined surfaces. Common reusable pallets are used to transport these components between several different machine processes. The pallet could be a generic rectangular container with a retroreflective surface on which an egg-crate-style transparent tray can be placed. This pallet design offers several advantages: (*1*) It reduces the application of retroreflective sheetings on individual trays to a minimum. (*2*) It allows flexibility to accommodate different part size without the needs to reapply retroreflective materials for new part change-over. (*3*) It allows different tray configurations to be interchangeable for use with the retroreflective container. Alternatively, nontransparent trays painted with retroreflective materials can be used. The use of retroreflective material as background eliminates

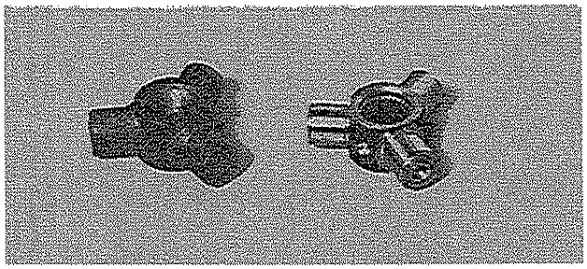

Fig. 14(*a*) Typical machine components

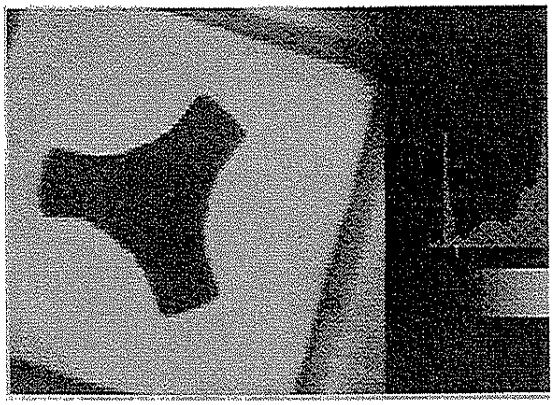

Fig. 14(*b*) Example of image of machine components

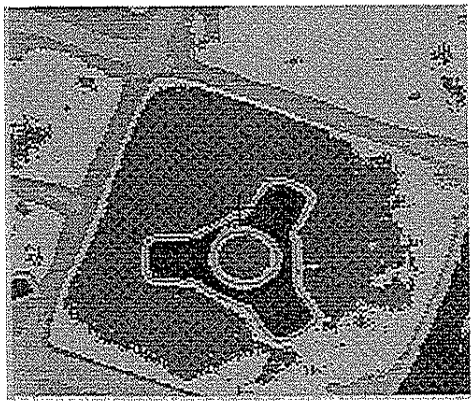

Fig. 14(*c*) Contour of digital image generated by pin-hole optics

the need for the active illumination source that would be required for back-lighting and thus significantly simplifies the design and maintenance of the resuable trays.

For relatively large components, the imaging sensor must be located at a considerable distance above the target plane in order to have a sufficiently large FOV as well as a reasonably uniform illumination. To avoid the prolonged exposure time required with the pin hole optic design I (a signed LED and beam splitter), a collocated illumination scheme similar to the optic design II was designed and constructed for concept demonstration. Eighteen narrow-angle LEDs were closely packed around a pin-hole of 0.1 mm diameter. The LEDs were arranged in hexagons of diameters of 6mm, 10mm, and 12mm. Due to the high reflectivity of the retroreflective materials, the simple optic allows low-power spectral source to faithfully produce a high object-to-background image for location and orientation computation as displayed in Fig. 14(*b*) and 14(*c*), where a relatively simple thresholding technique has been used to detect the outline of the part.

5 Conclusions

Pinhole optic design concepts for applications of retroreflection for part-presentation have been presented along with illustrative application. The concept of giving retroreflective materials an integral role in vision sensing for generic part-presentation has been proven to have significant potentials for improving vision realiability, reducing the computation, and lowering implementation cost for part-feeding applications.

The manner in which parts are fed to robots in an FMS depends on the nature of the manufacturing processes, the product design, and the material handling system as a whole. The analytical model, which characterizes the design parameters that influence the image quality, will aid establishing guidelines for part-design and packaging for high-performance part-feeding. It it expected that the results of this investigation will provide insight into the overall manufacturing system modeling, simulation, and guidelines for part-presentation equipment standardization.

Acknowledgment

This research is cosponsored by the Georgia Tech Material Handling Research Center (MHRC) and the National Science Foundation (NSF) through NSF Presidential Young Investigator Grant No. 8958383. Strong support from Dr. Ira Pence, MHRC Director, Dave Santo of GM, and Matt Orlson of Ford, is greatly appreciated.

References

1 Lee, K-M., and Li, D-R., 1991, "Retroreflective Vision Sensing for Generic Part-Presentation," MHRC Technical Report MHRC-TR-89-06. Presented at 1990 IEEE SouthCon/90, Orlando, Florida, March 20–22. Also in *Journal of Robotic Systems*, February, Vol. 7, No. 1.

2 Lee, K-M., 1990, "A Low-cost Flexible Part-Feeding System For Assembly Automation," *Proceedings of the ICARCV International Conference on Automation, Robotics and Computer Vision*, Singapore, September 18–21.

3 Lee, K-M., 1991, "Flexbile Part-Feeding System for Machine Loading and Assembly; Part I: A State-of-the-Art Survey; Part II: A Cost-effective Solution," the *International Journal of Production Economics*, Special Issue, December.

4 Federal Test Method Standard 370, 1977, "Instrumental Photometric Measurements of Retroreflective Materials and Retroreflective Devices, March 1.

5 Rennilson, J. J., 1980, "Retroreflective Measurements: A Review," *Applied Optics*, Vol. 19, No. 8, April, (A collection of five papers).

6 U.S. Department of Transportation, 1987, "Retroreflectivity of Roadway Signs for Adequate Visibility: A Guide," Final Report FHWA/DF-88/001, November.

7 Wargocki, F. E., Ray, A., and Hall, G. E., 1984, "Retroreflector Field Tracker," State-of-the-Art Imaging Arrays and Their Applications, SPIE Vol. 501, pp. 283–291.

8 Holcombe, W. D., Dickerson, S. L., Larsen, J. W., and Bolander, R. A., 1988, "Advances in Guidance Systems for Industrial Automated Guided Vehicles," *Proceedings of the SPIE-Mobile Robots III*, Cambridge, MA, November, 9–11.

9 Horn, B. K. P., 1986, *Robot Vision*, The MIT Press.

10 Optoelectronics Designer's Catalog, 1988–1989, Hewlett Packard, pp. 6-28, 6-31.

11 Laser Diode Product Catalog, Spectra Diode Labs, San Jose, CA 95134.

12 Xenon Flashtubes Catalog, Heimann Company.

13 Lee, K-M., Dickerson, S., and Mercurio, J., 1991, "Generic Retroreflective Part Pickup System (GRIPPS)," *Proceedings of the 1991 NSF Design and Manufacturing Systems Conference*, January 9–11, Austin, TX.